Characterizing Slight Structural Disorder in Solids by Combined Solid-State NMR and First Principles Calculations

Sylvian Cadars,[†,‡] Anne Lesage,[†] Chris J. Pickard,[§] Philippe Sautet,[||] and Lyndon Emsley*[,†]

CNRS/ENS Lyon/UCB-Lyon 1, Centre de RMN à Très Hauts Champs, Université de Lyon, 5 rue de la Doua, 69100 Villeurbanne, France, CEMHTI-CNRS: Conditions Extrêmes et Matériaux, Hautes Températures et Irradiation, 1D avenue de la Recherche Scientifique, 45071 Orléans cedex 2, France, School of Physics and Astronomy, University of St. Andrews, St. Andrews KY16 9AD, Scotland, and Laboratoire de chimie, CNRS and Ecole Normale Supérieure de Lyon, Institut de Chimie de Lyon, Université de Lyon, 46 allée d'Italie, 69364 Lyon, France

Received: November 18, 2008

A general approach for structural interpretation of local disorder in partially ordered solids is proposed, combining high-resolution two-dimensional (2D) nuclear magnetic resonance (NMR) and first principles calculations. We show that small chemical shift variations of the order of a ppm can be interpreted in detailed structural terms with advanced density functional theory methods. Focusing on a model system of bisphosphinoamine, we demonstrate that the existence and the spatial range of small amplitude disorder can be probed using quantitative statistical analyses of 2D NMR line shapes obtained from through-space correlation experiments collected using variable mixing times. We show how low-energy vibration modes calculated from first principles can be conveniently used not as a cause of disorder but, instead, to generate a basis set of physically plausible local distortions to describe *candidate* static distributions of local geometries. Calculations of ^{31}P NMR isotropic chemical shifts are then used for the first time to simulate 2D correlation lineshapes associated with these distortions, which permit their evaluation as a potential source of disorder by comparison to experimental 2D cross-peaks between phosphorus sites. This new type of structural constraints allows the identification of changes in the bonding geometry that most likely contribute to the local structural disorder. We thus identify at least one type of structural deformation that is compatible with the experimental 2D NMR data and is also within the order of magnitude of the "thermal ellipsoids" associated with the uncertainties on the atomic positions of the X-ray diffraction structure.

1. Introduction

Detailed characterization, at the molecular level, of structural disorder is an increasingly important challenge in materials science, biochemistry, or pharmaceutical industry, for example. Indeed, disordered systems are generally difficult to access using conventional characterization methods, such as diffraction techniques, which often rely on the existence of long-range atomic order. Nuclear magnetic resonance (NMR), on the other hand, has long been used for the study of disordered materials, since it allows the observation of the local chemical environment independently of the existence of long-range order.[1−4]

State-of-the-art multidimensional NMR correlation techniques in conditions of magic angle spinning (MAS) now offer many new opportunities to probe the local structure of noncrystalline solids, including the large range of inorganic systems involving quadrupolar nuclei (i.e., having a nuclear spin $I > 1/2$), whose intrinsic quadrupolar broadening can be removed by key technical (double rotation,[5] dynamic-angle spinning[6,7]) and multiple-pulse (multiple-quantum MAS,[8,9] satellite-transition MAS[10]) approaches. Many powerful multidimensional techniques derived from these methods emerged in the past decades (see, for example, refs 11−13 for recent general reviews), which have driven considerable progress in the understanding, at the molecular level, of disordered inorganic[14] (e.g., glasses[15−19]), hybrid,[20−22] or organic materials (e.g., biopolymers[23]).

In disordered solids where quadrupolar nuclei are not involved, the resolution of one-dimensional (1D) NMR spectra is also limited by broad distributions of isotropic chemical shifts resulting from the variations of local environments at each chemical site. The associated inhomogeneous broadening,[2,24] though typically smaller than quadrupolar lineshapes, often leads to partial overlap between the chemically different sites that complicate the interpretation of 1D NMR spectra. Advanced multidimensional NMR techniques can nevertheless be used to probe the local short-range order in noncrystalline solids through the differentiation of diverse molecular motifs up to the nanometer length scale[19,25] and may even overcome the resolution limits of 1D spectra through the observation (in favorable cases) of high-resolution two-dimensional (2D) correlation spectra.[26−31] This is typically the case in partially ordered materials[27] such as short-range ordered surfactant-templated layered silicates,[26,28] for example, in which the origins of small-amplitude structural disorder can be investigated through the analysis of 2D correlated NMR lineshapes with statistical methods[29] to extract the underlying (potentially extremely rich) structural information.[29,31,32] (We note that similar resolution enhancements in 2D as compared to 1D NMR spectra are commonly observed independently of the presence or absence of substantial structural disorder in solids subject to inhomogeneous broadening from anisotropic bulk magnetic susceptibil-

* Corresponding author. E-mail: lyndon.emsley@ens-lyon.fr.
[†] Centre de RMN à Très Hauts Champs, Université de Lyon.
[‡] CEMHTI-CNRS.
[§] University of St. Andrews.
[||] Institut de Chimie de Lyon, Université de Lyon.

10.1021/jp810138y CCC: $40.75 © 2009 American Chemical Society
Published on Web 01/09/2009

ity (ABMS),[2,33] or from bulk paramagnetic susceptibility in the presence of a paramagnetic center.[34,35]).

However, because the structural information contained in the 2D NMR lineshapes is encoded in terms of isotropic chemical shifts, the link with structural features is difficult to establish. Thus, detailed interpretations of the 2D NMR lineshapes of disordered systems in the form of distributions of local bonding geometries (e.g., bond angles, dihedral angles, etc.), for example, have remained particularly scarce[36,37] and mostly limited to the use of lineshapes resulting from anisotropic interactions (quadrupolar broadening[38,39] or chemical shift anisotropy in oriented samples[40,41]). Ab initio or first principles (i.e., DFT) calculations have recently appeared as valuable means of establishing the missing link between the variations of the local structure associated with disorder and experimental distributions of isotropic chemical shifts. In the past decade, much progress has indeed been made in the accurate prediction of chemical shifts in the solid state from first principles,[42−45] in particular. Except for a few notable examples,[36,37,46] however, DFT calculations of isotropic NMR chemical shifts have mainly focused on identifying different chemical sites, rather than interpreting small changes of isotropic chemical shifts (of the order of a ppm or so) within a single chemical site in detailed structural terms.

Here we propose a general approach for the structural interpretation of small amplitude local disorder in partially ordered solids, which combines high-resolution 2D nuclear magnetic resonance and first principles calculations. Through the example of a model system of bisphosphinoamine, we show how statistical analyses of 2D NMR lineshapes obtained from through-space correlation experiments collected using variable mixing times can be used to unambiguously identify the presence of static disorder and to probe its spatial range. Furthermore, we show how low-energy vibration modes calculated from first principles can be conveniently used to generate a basis set of physically plausible local distortions as candidates for describing the static distributions of local geometries that are responsible for the disorder. These low frequency modes are not considered as a cause or a source of disorder but indicate instead deformations associated with the lowest energy distortions that the molecules could potentially undergo as a result of external stresses such as packing, for example. Calculations of NMR ^{31}P isotropic chemical shifts are then used to predict the 2D ^{31}P−^{31}P correlation lineshapes associated with each candidate distortion thus obtained, which are then compared to the experimental 2D lineshapes. This novel type of structural constraints based on 2D isotropic chemical shift distributions between correlated sites allows the identification of complex distortions (i.e., involving concerted changes of several bond and/or dihedral angles) of the local bonding geometry that likely contribute to the structural disorder.

2. Experimental Section

2.1. Description of the Sample. The sample used for this study is *N*,*N*-bis(diphenylphosphino)-*N*-((*S*)-α-methylbenzyl)amine (**1**). It was synthesized in the Laboratoire d'Etudes Dynamiques et Structurales de la Sélectivité (Grenoble, France) as a π-acceptor bidentate ligand of a dicobalt complex, which has been studied as a candidate of the asymmetric Pauson−Khand reactions,[47,48] for which this class of ligands turned out to provide improved reactivity as well as slight final enantiomeric excess.

2.2. NMR Spectroscopy. The ^{31}P{^{1}H} CP-MAS spectrum was obtained on a Bruker Avance 700 standard bore spectrometer operating at ^{1}H and ^{31}P frequencies of 700.13 and 283.42 MHz, respectively, using a 2.5 mm double resonance probe at a MAS frequency of 32 kHz. Polarization transfer from ^{1}H to ^{31}P was achieved with a contact time of 2 ms using an adiabatic shape on the proton channel.[49] The SPINAL64[50] scheme at a proton nutation frequency of 125 kHz was used for heteronuclear decoupling.

The proton-driven ^{31}P−^{31}P spin-diffusion experiments were recorded on a Bruker Avance 500 wide bore spectrometer operating at ^{1}H and ^{31}P frequencies of 500.1 and 202.5 MHz, respectively, using a 2.5 mm double resonance probe. The MAS frequency was set to 9 kHz, and SPINAL64 proton decoupling at the nutation frequency of 140 kHz was applied during evolution and detection periods. A total of 256 points were acquired in the indirect dimension, within 16 transients. Cross polarization from protons to ^{31}P nuclei was achieved using a ramp on the proton channel and a contact time of 2 ms.

Extraction of conditional probability matrices, and calculation of chemical shift correlation coefficients from 2D homonuclear correlation spectra, were achieved by using a homemade Matlab routine that is available upon request to the authors.[29,31] This procedure has also recently been implemented in the matNMR toolbox of J. D. Van Beek.[51]

2.3. Computations. Gas-phase geometry optimizations, calculations of ^{31}P NMR shieldings, and frequency calculations were carried out at the density functional level of theory (DFT) using Gaussian 03[52] and the B3 hybrid exchange[53] functional, together with the PW91 correlation[54] functional for NMR calculations, and with the LYP[55] correlation functional for geometry optimizations and frequency calculations. Standard 6−31G* basis sets were used for all of the geometry optimizations and frequency calculations, and the more demanding chemical shift calculations (in terms of atom core description in particular) were achieved using locally dense basis sets, made of IGLO-III[56] for phosphorus and nitrogen atoms and IGLO-II for carbon atoms, while the 6−31G basis was kept for hydrogen atoms. Parameters for the IGLO-II and IGLO-III basis sets were obtained from the Basis Set Exchange program[57,58] of the Environmental and Molecular Sciences Laboratory.

First principles calculations in periodic boundary conditions were achieved using the CASTEP code,[59,60] which relies on a plane-wave-based DFT approach. The electron correlation effects are modeled using the PBE generalized gradient approximation.[61] For the geometry optimization we employed "ultrasoft" pseudopotentials[62] and a planewave cutoff energy of 392 eV. The unit cell parameters, namely (8.961, 16.663, 18.080 Å) and (94.83, 95.82, 93.23°) were taken from the XRD structure and kept fixed during the optimization. A 3 × 2 × 1 Monkhorst−Pack[63] grid was used to sample the Brillouin zone. The NMR calculations were performed using the Gauge Including Projector Augmented Wave approach (GIPAW),[42] at the same cutoff energy of 392 eV. This method allows for a full solid-state treatment of the system under investigation.

To avoid any unnecessary errors, the calculated shifts were arbitrarily referenced by fitting the calculated shieldings as a function of the experimental shift value by a straight line of slope −1 (the intercept thus being the only variable). The reference value is then extracted from the intercept of the best fit. This requires, of course, preliminary assignment, which was proposed from first principles calculations discussed further below.

3. Results and Discussion

3.1. Structural Disorder in "Crystalline" Solids. Our first objective is to characterize the presence and extent of disorder in polycrystalline *N*,*N*-bis(diphenylphosphino)-*N*-((*S*)-α-meth-

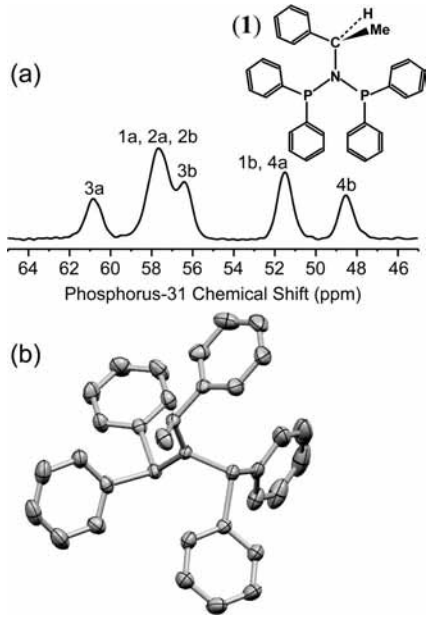

Figure 1. (a) Planar formula of *N*,*N*-bis(diphenylphosphino)-*N*-((*S*)-α-methylbenzyl)amine (**1**), along with the corresponding $^{31}P\{^{1}H\}$ CP-MAS spectrum, recorded at 16.44 T and at a MAS frequency of 32 kHz. The asymmetric unit contains four conformationally distinct molecules, which give rise to eight inequivalent (albeit partially overlapping) ^{31}P sites. (b) Residue 1 extracted from the X-ray structure of **1**, with the thermal ellipsoids representing the isosurfaces of 40% presence probability.

ylbenzyl)amine (**1**), which we consider as a model system for this type of study, and whose structure is shown in Figure 1a, to illustrate a general approach for the detailed examination of slight structural disorder in partially ordered molecular solids. The bisphosphinoamine (**1**) is a crystalline material in the common sense of the term, meaning that it has well-defined wide-angle X-ray reflections, from which a crystal structure could be determined.[64] The XRD structure has four molecules with distinct conformations per unit cell, each of which contains two phosphorus atoms, giving rise to eight ^{31}P NMR resonances, some of which are overlapped, as shown in the $^{31}P\{^{1}H\}$ CP-MAS spectrum shown in Figure 1a but which can be fully resolved using 2D $^{31}P-^{31}P$ correlation spectroscopy.[27]

Despite the high degree of long-range molecular order that yields well-defined XRD reflections, the ^{31}P NMR resonances of **1** are generally broad (typically ca. 1 ppm full width at half-maximum, fwhm), and yield remarkably elongated lineshapes in 2D NMR (see ref 27 or Figure S1). These lineshapes are the signature of distributions of isotropic frequencies associated with each crystallographic ^{31}P site, and they have previously been attributed to some extent of slight structural disorder,[27,29,30] or possibly to ABMS.[27] The observation of static disorder is in apparent contradiction with the XRD structure of **1**, which shows no disorder in the crystallographic sense of the term, i.e., all of the atoms are associated with well-defined crystallographic positions.[64] However, the XRD analysis shows uncertainties on the atomic positions, as expressed by the B-factors, which are usually interpreted as the thermal agitation of a given atom in the course of the XRD experiment (of the order of hours), and are referred to as dynamic disorder. Such fluctuations in the positions of the atoms are typically represented by ellipsoids, which correspond to isosurfaces of probability of presence, as shown for example for Residue 1 (at 40% probability) in Figure 1b. Specifically, the thermal ellipsoids suggest in this case a substantial freedom of rotation around the C−P, the P−N, and the N−C bonds. Here we will show that what is often considered as thermal motion may in some cases correspond, on the NMR time scale (i.e., 10^{-2} to 10^{-1} s), to *static distributions of slightly distorted structures*, and we propose a general strategy for the detailed interpretation of this slight static disorder using isotropic chemical shifts, by combining 2D correlation NMR spectroscopy and first principles calculations.

3.2. First Principles Studies of the Crystal Structure. A prerequisite step for the detailed structural analysis of solids is the assignment of the distinct NMR resonances to the different crystallographic sites. In the case of **1**, the eight ^{31}P NMR peaks have previously been classified in four $^{31}P-N-^{31}P$ pairs corresponding to the four conformationally distinct residues of the crystal structure using through-bond double-quantum (DQ) ^{31}P NMR,[27] specifically the refocused INADEQUATE experiment.[65] In this section, we use first principles calculations of NMR chemical shifts with periodic boundary conditions to propose a complete assignment of the eight ^{31}P NMR resonances to the crystallographic sites of **1**.

In recent years, first principles calculations of NMR parameters have been increasingly used in combination with solid-state NMR (see, for example, refs 37, 66−78). This rapidly growing interest has been driven in particular by the emerging potential offered by the introduction of accurate chemical shift calculations with periodic boundary conditions,[42,45] using plane-waves and pseudopotentials in the DFT code CASTEP,[59,60] which allows for integration of the long-range molecular environment of solids at low computational cost. It has been established that geometry optimization of published X-ray coordinates, and in particular the position of H atoms, is a prerequisite for reliable chemical shift calculations.[79] Figure 2a shows the superposition of the XRD structure (in red) and a fully relaxed structure optimized using CASTEP (in blue) with the unit cell parameters kept fixed (which will be referred to in the following as the "AllOpt-CL" structure, where "CL" is for "in the crystal lattice"). Hydrogen atoms have been hidden for clarity in this figure. Only very slight differences are observed between the two structures, as expressed by a heavy atom root-mean-square deviation (rmsd) of 0.039 Å (and an rsmd including H atoms of 0.118 Å) ($\text{rmsd} = \sum_{i=1}^{N} (x_{\text{opt},i} - x_{\text{XRD},i})^2/(3N)]^{1/2}$, where $i = 1...N$ designates the atoms, and $x_{\text{opt},i}$ and $x_{\text{XRD},i}$ are the Cartesian coordinates of the atom i in the XRD, AllOpt-CL structures, respectively). Despite these small differences, the geometry optimization with periodic boundary conditions provides significant improvement of the calculated chemical shifts, as compared to the XRD structure with only the H atoms relaxed, and allows complete assignment of the eight ^{31}P NMR resonances.

A convenient way of assigning the ^{31}P NMR signals to the distinct crystallographic sites consists of comparing the positions of the 2D $^{31}P-N-^{31}P$ correlation cross-peaks as observed in the refocused INADEQUATE experiment[65] reported in refs 27 or 29 (shown as black open circles in Figure 2b) with the cross-peak positions predicted from first principles calculations. The cross-peak positions reported in this figure correspond to single-quantum−double-quantum (SQ-DQ) correlations, where the cross-peaks associated with two correlated sites appear at the same frequency in the indirect (vertical) dimension, namely at the sum of their individual shifts. First principles calculations of NMR chemical shifts carried out with CASTEP on the XRD structure where only hydrogen atoms were allowed to relax ("Hopt-CL" structure) are reported as yellow squares in Figure 2a. They allow the unambiguous assignment of the pair of $^{31}P-N-^{31}P$ cross-peaks at ca. 99 ppm in the DQ (vertical)

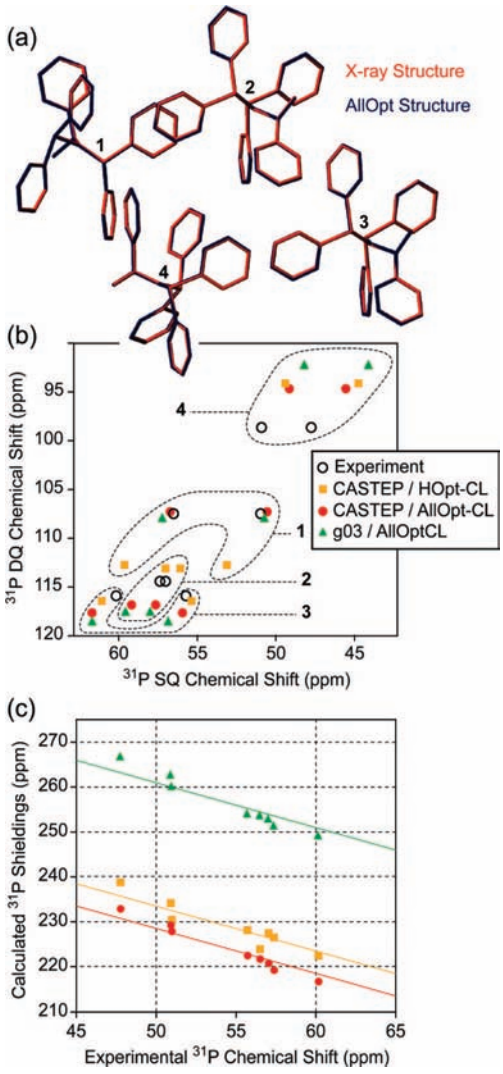

Figure 2. (a) Superposition of the X-ray structure of **1** (in red) and the structure relaxed using CASTEP ("AllOpt-CL", in blue), with cell parameters kept frozen. The position of the four N atoms was matched for comparison, and the average rmsd was 0.039 Å, excluding the H atoms, which are not shown for clarity in this figure. (b) Comparison of different calculated SQ-DQ spectra with positions of experimental cross-peaks (open black circles), as obtained previously.[27,29] Red circles correspond to a CASTEP calculation on the AllOpt-CL structure. Yellow squares correspond to the CASTEP calculation with only the H atoms relaxed (HOpt-CL). Green triangles were obtained considering every residue of the AllOpt-CL structure in isolation with Gaussian 03. The assignment was proposed on the basis on this figure and is indicated by the dashed-line areas and corresponding labels. (c) Same data as in b shown as correlation plots between the experimental ^{31}P shifts and the calculated shieldings, using the same color code as in b. The solid lines correspond to the best fits of each data set to a straight line with an imposed slope of −1.

dimension to Residue 4 in the crystal structure (see Table 1). Good agreement is also found between the pairs of cross-peaks at ca. 114 and ca. 116 ppm in the DQ dimension with the calculated chemical shifts of Residues 2 and 3, respectively. Some ambiguity nevertheless persists at this point since the cross-peak positions predicted for Residue 1 differ significantly from the remaining pair of ^{31}P−N−^{31}P cross-peaks at ca. 108 ppm in the DQ dimension. In contrast, similar chemical shift calculations carried out with CASTEP on the fully relaxed structure ("AllOpt-CL") shows substantially improved agreement for the predicted cross-peak positions of Residue 1, thereby confirming unambiguously the assignment of the eight ^{31}P resonances to the eight distinct crystallographic sites suggested by the calculations carried out on the Hopt-CL structure. This assignment is given in Table 1 and is indicated on the ^{31}P{^{1}H} CP-MAS spectrum of Figure 1a. The only possible ambiguity that remains, of little relevance in the analysis of the disorder that is the main focus of this work, concerns the assignment of the two ^{31}P resonances 2a and 2b associated with Residue 2, which have very close frequencies (57.4 and 57.0 ppm). We are nevertheless confident that the assignment proposed for this pair in Table 1 (namely the ^{31}P resonances 2a at 57.4 ppm and 2b at 57.0 ppm attributed to P atoms 4 and 3 of the XRD structure, respectively) is correct, based on the previous observations that first principles calculations using CASTEP generally predict accurate signs of the chemical shift differences between pairs of even slightly inequivalent sites.[72,75] On the basis of this assignment, the same data has been reported in a more conventional way (Figure 2c), as a correlation plot between calculated shieldings and experimental chemical shifts. The improved agreement between experiment and calculations upon geometry optimization in periodic boundary conditions is similarly reflected in this plot, with smaller deviations from the ideal −1 correlation (solid lines) for CASTEP calculations carried out on the AllOpt-CL structure (red circles) (rmsd of 1.33 ppm) as compared to calculations performed on the HOpt-CL structure (yellow squares) (rmsd of 1.88 ppm) (Here, rmsd $= [\sum_{i=1}^{N} (\sigma_{\mathrm{calcd},i} - \sigma_{0,i})^2/N]^{1/2}$, where $i = 1...N$ designates the ^{31}P nuclei, $\sigma_{\mathrm{calcd},i}$ is the calculated isotropic shielding for i, and $\sigma_{0,i}$ is the shielding given by the best fit of the series of calculated shieldings to $\sigma_{0,i} = -\delta_i + a$ (solid lines in Figure 2c)).

To understand in more detail the structural features that account for the relative positions of the different NMR resonances, chemical shift calculations were finally carried out on each residue of the AllOpt-CL structure considered in isolation (i.e., in the gas phase), using Gaussian 03.[52] The SQ-DQ cross-peak positions thus predicted have been represented as green triangles in figures 2b and 2c and show very similar trends as those observed from the CASTEP calculations carried out on the same structure (red circles) in the full crystalline environment, with an acceptable rmsd of 1.95 ppm. This suggests that, in the particular case of **1**, inter-residue electronic effects have little influence on relative chemical shifts of the different crystallographic ^{31}P sites, despite the presence of a large number of phenyl rings in the structure, whose long-range effects on chemical shifts are well-known.[80,81] Hence, the local structure around the two phosphorus atoms in each molecule controls the relative ^{31}P chemical shifts in this system. Here, the main advantage of calculations using periodic boundary conditions is thus to account for the stabilization of the different residues in their respective crystallographic conformation by steric effects.

3.3. Nature, Spatial Range, And Quantification of the Structural Disorder. With the complete assignment of the ^{31}P NMR resonances of **1** to the different crystallographic sites, we can now turn our attention to the more subtle effects that are responsible for the distributions of isotropic chemical shifts and the associated elongated ^{31}P−^{31}P cross-peaks in 2D NMR spectra.[27,29] Specifically, in addition to the slight static structural disorder within the uncertainties of the XRD structure that has been hypothesized, several effects can potentially account for the elongation of the ^{31}P−^{31}P correlation lineshapes parallel to the diagonal, such as ABMS broadening,[27,33,35] or the second-order dipole−quadrupole interaction between the ^{31}P nuclei and the quadrupolar ^{14}N nuclei (nuclear spin $I = 1$, natural abundance of 99.6%).[82] The latter effect is expected to induce

TABLE 1: Complete Assignment of ^{31}P NMR Signals to the Crystallographic Sites

residue no.[a]	P atoms	XRD label[a]	calcd ^{31}P chemical shift (ppm)[b]	exptl ^{31}P chemical shift (ppm)[c]	exptl DQ chemical shift (ppm)[c]	assignment
1	1	56.7	56.5	107.5		1a
	2	50.6	51.0			1b
2	3	57.7	57.0	114.4		2b
	4	59.2	57.4			2a
3	5	55.9	55.7	115.9		3a
	6	61.7	60.2			3b
4	7	49.1	50.9	98.6		4a
	8	45.5	47.7			4b

[a] As in ref 64. [b] From CASTEP, after full optimization in periodic boundary conditions. [c] Position of the center of mass (with uncertainties of ca. ± 0.1 ppm) of the cross-peaks of a 2D refocused INADEQUATE spectrum recorded at 11.74 T, 32 kHz MAS, at ambient temperature,[30] and referenced to 85% phosphoric acid (at 0.0 ppm).

a splitting of each individual ^{31}P resonance as a result of the proximity to the nearby ^{14}N nucleus under MAS, which can be calculated from the electric field gradient tensor and the internuclear distance.[82] In the particular case of **1**, we predict splittings of less than ca. 80 Hz at 11.74 T using DFT calculations of the electric field gradient (see details in Supporting Information), i.e., less 0.4 ppm as compared to observed experimental ^{31}P resonances of full width at half-maximum (fwmh) of about 1.0 ppm. Although this is obviously a significant effect, it does not account for the broadening. This is especially true at higher magnetic fields, since the second order dipole−quadrupole interaction scales with the inverse of the magnetic field. For example, similar elongated 2D NMR lineshapes were also observed at 16.44 T (data not shown) despite predicted splittings of individual ^{31}P resonances of less than 0.2 ppm (less 60 Hz at 16.44 T, see Supporting Information). Thus, since **1** is used here as a model system to present a general strategy for the characterization of the structural disorder in partially ordered solids, we chose to neglect the potential contribution of the second-order dipole−quadrupole interaction below.

Potential contributions from ABMS, on the other hand, can be probed by examining the spatial range of the interactions that are responsible for the elongated 2D NMR lineshapes. Here, we use through-space correlation spectroscopy to demonstrate the short spatial range of the effects that account for the elongated 2D ^{31}P−^{31}P correlation lineshapes, which are thereby unambiguously attributed to small amplitude local structural disorder. By definition, ABMS effects have a long range, of the order of crystallite dimensions, and would yield identical peak elongation along the diagonal axis (in ppm) for any type of correlation spectrum (e.g., homo- or heteronuclear, through-bond or through-space correlation experiment). Specifically, series of 2D ^{31}P−^{31}P proton-driven spin-diffusion (PDSD) experiments were recorded with mixing times τ_M ranging from 20 ms to 2 s (see Figure S1, Supporting Information for the whole series of spectra), during which through-space magnetization exchange between phosphorus atoms a few angströms apart can occur, resulting in off-diagonal correlation peaks. At short mixing times τ_M, essentially intraresidue correlations Xa-Xb, with $X = 1$, 2, 3, or 4, across the short (<3.0 Å) ^{31}P−N−^{31}P distances are present, as illustrated for $\tau_M = 100$ ms in Figure 3a. For longer mixing times, additional cross-peaks appear that are unambiguously assigned to *purely inter-residue correlations*, as is the case for $\tau_M = 2$ s (Figure 3b). Interestingly, the elongated profile of the intraresidue correlation peaks observed at short spin-diffusion mixing times disappears when longer-range inter-residue correlations are present. This not only rules out contributions from ABMS but more importantly is a clear indication that the interactions that are responsible for the elongated ^{31}P−^{31}P lineshapes observed so far (Figure 3a and refs 27, 29, 30) have a strictly local character.

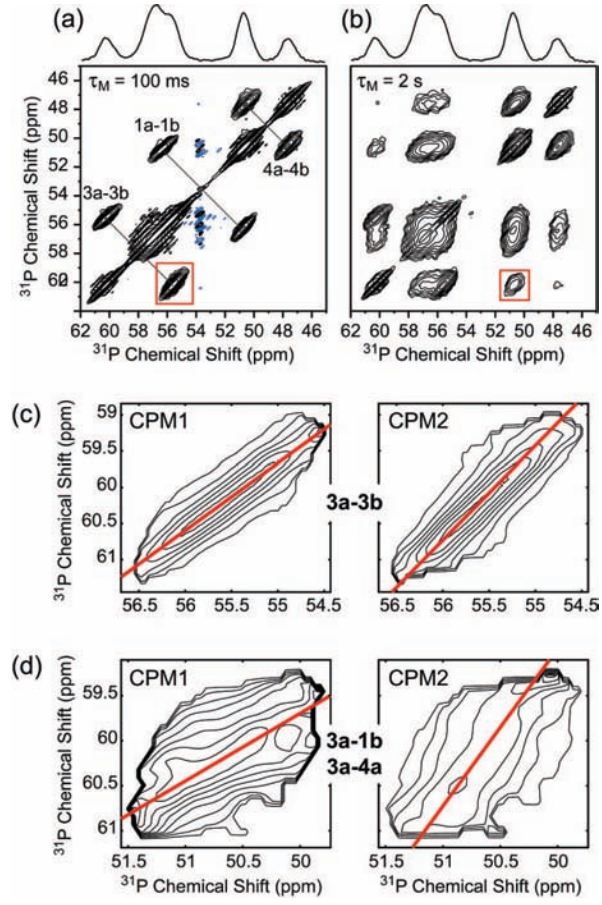

Figure 3. (a, b) NMR proton-driven ^{31}P−^{31}P spin-diffusion spectra recorded with spin-diffusion mixing times of (a) 100 ms and (b) 2 s, in otherwise identical conditions (11.74 Telsa, at a MAS frequency of 9 kHz). (c) Pair of conditional probability matrices CPM1 and CPM2 extracted from the purely intraresidue 3a-3b cross-peak outlined in a, and obtained with a spin-diffusion mixing time of 100 ms. (d) Pair of conditional probability matrices CPM1 and CPM2 extracted from the long-range inter-residue cross-peak outlined in b, which is a mixture of 3a-1b and 3a-4a correlation, for a spin-diffusion mixing time of 2 s. The red lines in c and d correspond to the best fits of maximum intensities in the CPM1 and CPM2 matrices to straight lines, from which the r_{AB} correlation coefficients were extracted (see Supporting Information).

Specifically, more detailed information on the spatial range of the disorder can be obtained from quantitative analyses of the ^{31}P−^{31}P cross-peaks obtained at various spin-diffusion mixing times. In particular, we recently discussed statistical analyses based on conditional probability distributions that can

TABLE 2: Chemical Shift Correlation Coefficients Extracted from $^{31}P-^{31}P$ PDSD Experiments with Spin-Diffusion Mixing Times of 100 ms and 2 s

spin-diffusion mixing time (s)	cross-peak position (ppm)	assignment (s)	intraresidue distance (Å)	inter-residue distances (Å)[a]	r_{AB} correlation coefficients[b,c]	ρ_{AB} correlation coefficients[c]
0.1	(60.2, 52.4)	3a-3b	2.97	6.0	0.87 ± 0.03	0.79 ± 0.01
	(56.2, 50.8)	1a-1b	2.98	8.1	0.89 ± 0.01	0.82 ± 0.01
	(50.6, 47.5)	4a-4b	2.97	6.0	0.77 ± 0.01	0.72 ± 0.01
2.0	(60.3, 50.6)	3a-1b	–	10.2	0.62 ± 0.04	0.48 ± 0.00
		3a-4b	–	9.5, 10.9		
	(50.6, 47.5)	4a-4b	2.97	6.0	0.58 ± 0.10	0.52 ± 0.01
		4a-1b	–	8.4, 9.8, 11.0		
	(60.2, 47.5)	3a-4b	–	8.9, 9.1, 10.9	0.6[d]	0.4[d]

[a] Cutoff value of 11.0 Å. [b] Calculated as in ref 31; see Supporting Information. [c] Uncertainties correspond to the difference between similar coefficients calculated from the two symmetric cross-peaks of a given PDSD spectrum. [d] Calculated from one cross-peak only, since the second had too low intensity.

be extracted from 2D correlation peaks.[29] For example, Figure 3c shows the pair of conditional probability matrices CPM1 and CPM2 that can be extracted (see details in Supporting Information) from the 3a-3b correlation peak at (60.2, 55.5 ppm) in the PDSD experiment recorded with $\tau_M = 100$ ms (outlined in Figure 3a). The intensity of a point CPM1(ω_{3a}^k,ω_{3b}^l) of the conditional probability distribution CPM1 yields the probability that ^{31}P site 3a resonates at ω_{3a}^k given that ^{31}P site 3b resonates at ω_{3b}^l. Similarly, the intensity CPM2(ω_{3a}^k,ω_{3b}^l) of the conditional probability distribution CPM2 gives the probability that site 3b resonates at ω_{3b}^l given that site 3a resonates at ω_{3a}^k.[29] (The conditional probability distributions CPM1 and CPM2 thus only differ by the information that is considered known, namely the resonance frequency of site 3b or site 3a, respectively.)

The comparisons of the conditional probability distributions extracted from intraresidue and inter-residue correlations from the PDSD experiments recorded for $\tau_M = 100$ ms (Figure 3a) and $\tau_M = 2$ s (Figure 3b), respectively, show remarkable differences. Specifically, the elongated intraresidue 3a-3b cross-peak highlighted in Figure 3a yields CPM1 and CPM2 matrices with nearly parallel profiles (Figure 3c), indicating a high degree of chemical shift correlation between these two sites. By comparison, the significantly broader inter-residue cross-peaks observed at longer mixing times yield pairs of conditional probability distributions CPM1 and CPM2 with substantially different profile directions, as illustrated in Figure 3d by the probability distributions extracted from the (degenerate) 3a-1b and 3a-4a correlation peaks highlighted in Figure 3b. On the basis of the observation of similar variations in the relative profiles of pairs of conditional probability matrices in different systems, we have shown[31] that the *degree of local order* can be quantified through the extraction of coefficients expressing the degree of chemical shift correlation r_{AB} between to sites A and B. These coefficients vary between 0 and 1, where 0 corresponds to a total absence of chemical shift correlation between the two sites, whereas $r_{AB} = 1$ indicates a perfect linear correlation. A series of these chemical shift correlation coefficients r_{AB} were extracted from the different $^{31}P-^{31}P$ correlation peaks obtained for $\tau_M = 100$ ms and 2 s, and they are reported in Table 2 along with the assignments to either or both intraresidue and/or inter-residue correlations, and the associated P−P distances extracted from the crystal structure. At short spin-diffusion mixing times, high degrees of chemical shift correlation r_{AB} are observed for all cross-peaks (between 0.77 and 0.89), which result from essentially intraresidue correlations (P−P distances of less than 3.0 Å), with potentially only small additional contributions from inter-residue correlations between for example a ^{31}P site Xa and the ^{31}P site Xb ($X = 1$, 3, or 4) in an adjacent unit cell (P−P distances of between 6.0 and 8.1 Å depending on the residue). The degree of chemical shift correlation dramatically decreases when longer-range correlations are considered, at spin-diffusion mixing times of 2 s, as illustrated for example by r_{AB} values of ca. 0.6 for inter-residue correlations 3a-1b (and overlapping 3a-4b), or 3a-4b, which are associated with P−P distances of between 8.9 and 11.0 Å. We again note at this point that this excludes ABMS effects for source of broadening here, since long-range (by definition) ABMS would produce high correlation coefficients for all correlation peaks at all mixing times.

This significant decrease in the degree of chemical shift correlation, i.e., in the degree of local order, as a function of the internuclear distance is reflected even more clearly by extracting Pearson product-moment coefficients that are commonly used to quantify the degree of correlation between two variables.[83,84] The Pearson correlation coefficients ρ_{AB} between the chemical shift distributions of sites A and B also vary from 0 to 1 for increasing extents of correlation in the case of a positive correlation (high frequencies of one site correlate with high frequencies of the other site, and low frequencies correlate with low frequencies) and decrease between 0 and −1 for negative correlations (or "anti-correlations", i.e., correlations between high frequencies of one site and low frequencies of the other site), and can be extracted very easily from single-quantum−single-quantum (SQ-SQ) cross-peaks as detailed in Supporting Information. These Pearson chemical shift correlation coefficients ρ_{AB} were also extracted from the different cross-peaks of the PDSD spectra of Figure 3a and 3b, and show identical trends to the r_{AB} coefficients, since they decrease from between 0.72 and 0.82 for short-range intraresidue correlations to between 0.4 and 0.52 for long-range inter-residue correlations.

Using these quantitative analyses, it is then possible to follow the change in the degree of correlation, and thus the degree of order, reflected by a given 2D cross-peak when the spin-diffusion time increases, i.e., for increasing contributions of long-range correlations. For example, Figure 4 shows the r_{4a4b} (gray diamonds and gray error bars) and Pearson product moment ρ_{4a4b} (black squares and black error bars) coefficients extracted for the 4a-4b correlation peaks as a function of τ_M. This cross-peak is associated with an intraresidue P−P distance of 2.97 Å and an inter-residue distance of 6.0 Å, with additional contributions from the overlapping 4a-1b correlation at long mixing times (three P−P distances between 8.4 and 11.0 Å, see Table 2). Generally smaller Pearson coefficients ρ_{4a4b} are observed as compared to the r_{4a4b} coefficients, which is due to the fact that the procedure for extracting the r_{4a4b} coefficients focuses on the intensity maxima of the conditional probability distributions, which are thus more sensitive to the dominant short-range contribution, in contrast with the ρ_{4a4b} coefficients that integrate

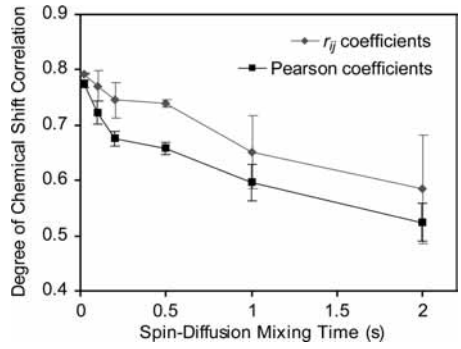

Figure 4. Chemical shift correlation coefficients associated with $^{31}P-^{31}P$ pair 4a-4b (50.9, 47.7 ppm) extracted from $^{31}P-^{31}P$ PDSD experiments at spin-diffusion mixing times ranging from 20 ms to 2s (see Supporting Information, Figure S1). Correlation coefficients calculated as described in ref 31 (r_{4a4b} coefficients) are displayed as gray diamonds and gray error bars. Pearson product-moment correlation coefficients ρ_{4a4b} are shown as black squares and black error bars. The error bars correspond to the difference between similar coefficients calculated from the two symmetric 4a-4b cross-peaks of a given PDSD spectrum.

the full 2D line shape. In both cases, however, a clear monotonic decrease of the degree of chemical shift correlation is observed for increasing mixing times, which is again consistent with a decrease of the degree of order with the internuclear distance. This supports the hypothesis that the disorder is due to structural variations within each molecule, which are already not (or poorly) correlated with the distortions of the next-nearest residues. This conclusion is consistent with previous observations of distributions of $^2J(^{31}P-N-^{31}P)$ scalar couplings in **1**.[30] Indeed, scalar couplings have a highly localized character, so that $^2J(^{31}P-N-^{31}P)$ coupling distributions are indicative of variations of the local bonding geometry around the P−N−P fragments across the sample. Furthermore, the essentially intraresidue range of the chemical shift correlations observed here rules out disorder due to variations in the periodic structures from one crystallite to the next or even from different several-nanometer-size (or above) domains within the crystallites. For the same reason, intermolecular effects such as chemical shift variations induced by distributions of orientations of aromatic rings in nearby residues,[81,85−87] for example, most likely only have minor contributions to the disorder in the present case. In summary, these results clearly reveal that this system exhibits static disorder in the conformations of its constituent molecules on the length scale of around 10 Å.

3.4. Structural Interpretations of the Disorder. Qualitative and quantitative approaches based on 2D NMR line shape analyses were proposed to probe the existence and the spatial range of the static structural disorder in the previous section. In the case of **1**, it becomes clear that the elongated 2D $^{31}P-^{31}P$ lineshapes are due to slight local structural distortions of the bonding geometry, for which structural interpretations will now be proposed using first principles calculations.

The number of degrees of freedom that can potentially account for the local structural disorder in a molecule such as **1** is enormous and includes strictly local distortions of individual angles as well as concerted distortions of several bond and dihedral angles and/or distances in the molecule. As a possible approach to this problem, in this section, we therefore propose to use low-energy vibration modes to *generate physically plausible basis sets of potential deviations from an average structure*. Such low-energy modes are thus not considered as a source or a cause of disorder but correspond instead to energetically favorable internal distortions of a given residue, which could be stabilized by intermolecular (essentially steric) interactions with surrounding molecules in the crystal, to lead to static disorder.

Since we have established (see section 3.3) that the disorder in **1** has an essentially intramolecular character (thereby ruling out intermolecular effects such as ring currents on nearby residues), basis sets of distortions generated by collective vibration modes of the lattice would not account for the disorder. On the other hand, low-energy vibration modes involving essentially local independent distortions of single residues could be used to describe the structural variations associated with the disorder. Chemical shift calculations could then be carried out for all ^{31}P sites on a series of modified structures generated along such intraresidue vibration modes. For each vibrational mode, the results would finally be shown as a series of superimposed predicted 2D spectra yielding 2D trajectories, i.e., predicted lineshapes, that could then be compared to the orientations of the experimental 2D cross-peaks (such as those of Figure 3a), thereby allowing the identification of structural distortions that are consistent with the observed disorder. Indeed, while a 1D chemical shift distribution is potentially consistent with virtually any local structural distortion, only a limited number of these low energy distortions may be consistent with the 2D distribution associated with correlated sites,[29] and, in the particular case of **1**, would reproduce the 1:1 linear correlations observed for $^{31}P-N-^{31}P$ pairs.

In practice, frequency calculations must be carried out on a fully relaxed (atomic positions and unit cell size and shape) crystal structure, where each molecule is found in a nonequilibrium geometry stabilized by its crystalline environment, principally through steric effects in the case of **1**. The crystalline environment is hence expected to influence the degrees of freedom of the molecule and thus the nature and the amplitude of even essentially intraresidue vibration modes, which, ideally, should consequently be calculated in the full solid-state environment with periodic boundary conditions. Unfortunately, because of the size of the system (256 atoms per unit cell) and of its large flexibility, were not able to calculate the vibrational modes of **1** using periodic boundary conditions. Nevertheless, our objective is to generate and test (using subsequent chemical shift calculations) plausible groups of structures, rather than to accurately describe the vibration modes of the molecule. Therefore, we used an alternative approach based on gas-phase frequency calculations.

Given the short spatial range of the disorder, and its essentially intramolecular character (see section 3.3), vibration modes calculated for molecules considered in isolation (i.e., in the gas phase) are expected to provide reasonably plausible sets of potential distortions, despite their neglecting intermolecular effects (e.g., ring currents from aromatic rings in neighboring residues, or variations of the hydrogen bonding network in other organic solids[87]) as a potential source of disorder. Moreover, we have also shown that chemical shift calculations carried out in the gas-phase yield good results provided the initial geometry has been optimized in the crystal (see section 3.2). As mentioned above, however, each residue of the AllOpt-CL structure, when considered in isolation, is found in a nonequilibrium geometry, on which gas-phase vibrational frequency calculation cannot be performed. Separate geometry optimizations were therefore carried out for each residue using Gaussian 03, yielding two distinct minimum-energy conformations, which we refer to as "AllOpt-GP-A" and "AllOpt-GP-B", as obtained from residues 1 and 4, and from residues 2 and 3, respectively. These two gas-phase-optimized structures essentially differ by the orienta-

tions of the phenyl rings and the torsion angle around the P−N bonds, with the conformation of AllOpt-GP-A being very similar to that of residue 1 of the crystal structure, whereas AllOpt-GP-B is more similar to the residues 2 and 3. (We note that the conformation of residue 4 in the crystal deviates substantially from that of both gas-phase optimized structures, and, in the following, the results obtained for this particular residue should be considered with care in consequence.)

Gas-phase frequency calculations were then carried out on optimized structures AllOpt-GP-A and AllOpt-GP-B, and the low-energy vibration modes, expressed in internal coordinates (i.e., distances, bond angles, and torsion angles), were subsequently applied to residue 1 and 4, and to residues 2 and 3, respectively, as optimized in the crystal (AllOpt-CL-X, with $X = 1, 2, 3,$ and 4). Defining $\mathbf{V}$ as the normalized distortion vector (in internal coordinates) associated with a given frequency mode of the gas-phase optimized structure, and $\mathbf{U}_0$ the internal coordinates of the solid-state optimized residue (using the exact same set of internal coordinate definitions), a series of distorted molecules of coordinates $\mathbf{U}(K)$ is obtained by applying the simple relation:

$$\mathbf{U}(K) = \mathbf{U}_0 + K\mathbf{V} \quad (1)$$

Calculations of ^{31}P chemical shifts are then carried out on the distorted structures with $\mathbf{U}(K)$ coordinates. The K values determine the sign and amplitude of the distortions and were chosen to yield calculated chemical shifts that roughly reproduce the experimentally observed chemical shift ranges (i.e., ^{31}P NMR peaks with fwhm of ca. 1 ppm) (To simplify the analyses and calculations of the internal distortions from a given vibrational mode, we only considered variations of bond angles and dihedral angles above arbitrary cutoff values for $K = 1$ of 0.4 and 1°, respectively, for the calculation of the distortion vector $\mathbf{V}$. Variations of bond lengths were not considered.)

For each residue, and for a few of the lowest energy vibration modes (arbitrarily chosen below 30 cm^{-1}), a set of distorted structures was generated (with $K = -2$ to 2), and the ^{31}P chemical shifts calculated for the two P atoms of each structure are reported in a 2D plot, representing the chemical shift of the ^{31}P site Xb as a function of the chemical shift of the ^{31}P site Xa ($X = 1, 2, 3,$ or 4). Each resulting plot corresponds to a predicted SQ-SQ intraresidue correlation peak (e.g., through-bond correlations, or through-space correlations obtained with short mixing times), and Figure 5 shows a few examples of these predicted cross-peaks, along with the corresponding set of distorted structures (shown as red, magenta, gray, cyan, and blue for $K = -2, -1, 0, 1, 2$, respectively). In each 2D plot, the 1:1 axis, which corresponds to the experimentally observed correlation axis from PSPD spectra obtained with short mixing times (Figure 3a), is shown as a gray dashed line. The closer the calculated trajectory is to the 1:1 axis, the higher the probability that the associated distortions provide a good representation of the local disorder in this system. For example the lowest gas-phase frequency mode obtained from AllOpt-GP-A ($E_{vib} = 13.7$ cm^{-1}) generates distortions of AllOpt-CL-1 (Figure 5a) that agree qualitatively well with the experimental chemical shift correlation. This suggests that similar distortions might be partially responsible for the structural disorder. This mode combines a distortion of the nitrogen pyramid, rotations around the N−P bonds, and slight rotations of the phenyl rings bonded to P1b. Here, distortions generated with $K = \pm 2$ (red and blue structures), although seemingly small in amplitude, result in ^{31}P chemical shift variations of ±2−5 ppm as compared to the original AllOpt-CL-1 structure (in gray). This is significantly greater than the observed broadening of the ^{31}P NMR resonances (fwhm of ca. 1 ppm), such that the actual amplitude of the disorder would be reproduced by K values in the −0.5 to 0.5 range. The corresponding distortions of the structure are

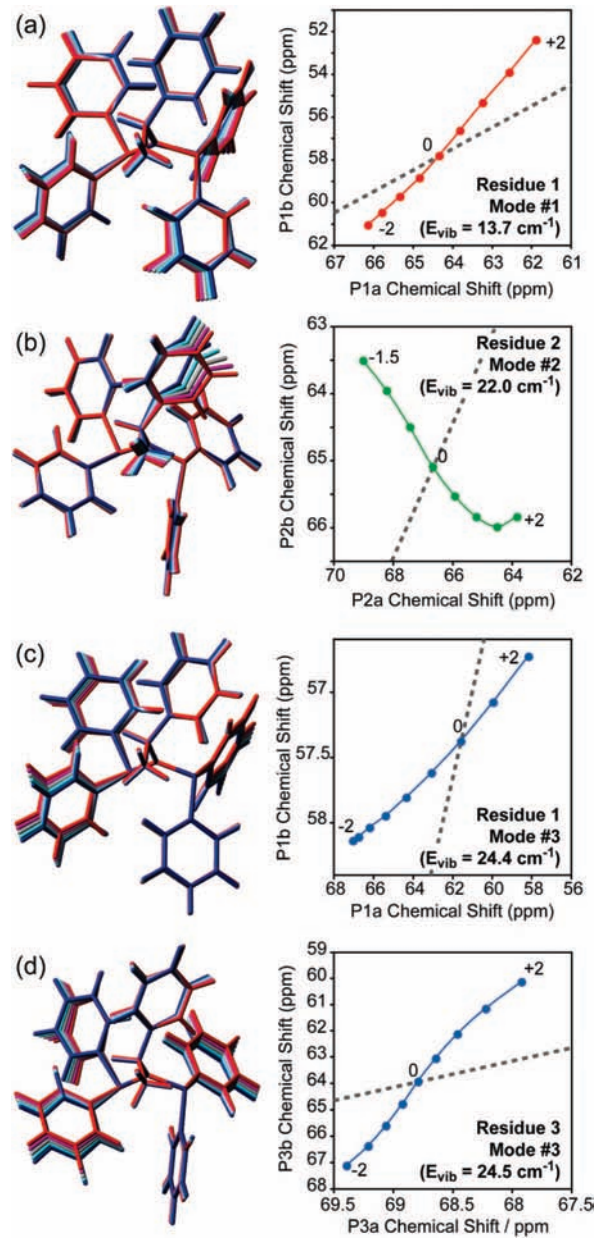

Figure 5. Series of ^{31}P−^{31}P chemical shift trajectories (i.e., predicted correlation peaks) calculated on series of structures generated along low-frequency vibrational modes (see text for details). The nondistorted structures ($K = 0$) correspond to the residues extracted from the AllOpt-CL structure. For each plot (right), the ensemble of structures considered is shown (left), with red, magenta, gray, cyan, and blue colors respectively corresponding to $K = -2, -1, 0, 1,$ and 2. The 1:1 axis associated with the experimental isotropic chemical shift correlation is indicated in each plot by the gray dashed line. Comparisons between the calculated correlation peaks and the 1:1 axis are used to determine whether a given set of distortions is compatible with the static structural disorder in **1**. (a) Calculations performed on the AllOpt-CL-1 structure, and the ensemble of distorted structures obtained from the lowest vibration modes obtained for AllOpt-GP-A. (b) Calculations performed on the AllOpt-CL-2, and distortions from the second vibration mode of AllOpt-GP-B. (c) Calculations performed on the AllOpt-CL-1, and distortions from the third vibration mode of AllOpt-GP-A. (d) Calculations performed on the AllOpt-CL-3, and distortions from the third vibration mode of AllOpt-GP-B.

small (e.g., within ±1−1.5° for the C−P−N−P dihedral angles defining the rotations of the phenyl rings about the P−N bonds, within ±1−2° for the C−C−P−N dihedral angles defining the rotations of the phenyl planes about the C−P bonds, and within ±0.2° for the P−N−P bond angle, etc.) and typically in the range of the thermal ellipsoids (Figure 1b), as hypothesized in Section 3a, and are thus compatible with the X-ray structure.

Nevertheless, this vibration mode has no equivalent in the four lowest frequency modes obtained from AllOpt-GP-B and was not considered for Residues 2 and 3. Neither is this mode in agreement with the experimental chemical shift correlations when applied to Residue 4 (which may not be surprising considering the particular conformation of this residue).

That this procedure generates very strong structural constraints for the identification of the distortions potentially reproducing local disorder is demonstrated by considering the distortions generated for AllOpt-CL-2 along the second vibration mode (E_{vib} = 22.0 cm^{-1}) calculated for AllOpt-GP-B, as shown in Figure 5b. *The associated distortions, which principally correspond to rotations around the C−N bond, can be immediately excluded as a source of structural disorder* for Residue 2, since they yield an anticorrelation between the two P atoms, in clear disagreement with the experiment. Yet, it is important to note that such distortions would perfectly well reproduce the 1D spectrum, since it is associated with similar variations *in magnitude* of both ^{31}P nuclei. Similar anticorrelations were found for this vibration mode applied to AllOpt-CL-3 and for the equivalent vibration mode calculated from AllOpt-GP-A and applied to residues 1 and 4, which confirms that the associated rotations around the N−C bond of each residue do not contribute to the disorder in **1**. Finally, we found that the third vibration mode (E_{vib} = 24.4 and 24.5 cm^{-1} for AllOpt-GP-A and B, respectively) yields calculated ^{31}P−^{31}P trajectories reasonably close to the experimental 1:1 correlation for all residues (as shown in Figure 5c and 5d for AllOpt-CL-1 and AllOpt-CL-3, respectively). These distortions, which principally correspond to concerted variations of the torsion angles around both P−N bonds (of ± 1−1.5° for $K = \pm 0.5$, corresponding to chemical shift variations of the two correlated ^{31}P nuclei the order of ±1 ppm), are thus also likely candidates for reproducing the main sources of local structural disorder in the bisphosphinoamine **1**. In summary, our purpose here was not to equate vibrational modes with disorder, and we have only considered a small number of modes (here the smallest three). The objective is to find distortions that can involve many bonds, angles, and geometries and which are both plausible and compatible with the experimental data. This approach appears to be validated here, since we see that some distortions are clearly incompatible with the strong constraints provided by 2D NMR isotropic chemical shift distributions between correlated sites, while at least one of the distortions (involving several concerted variations of dihedral angles in particular) does reproduce qualitatively the trends observed with small amplitude structural variations that are compatible with the X-ray structure.

4. Conclusions

By combining high-resolution NMR chemical shifts in disordered solids and first principles calculations, we have shown how an in-depth analysis of slight structural disorder in partially ordered materials can be achieved. The presence and the spatial range of the disorder can be probed using quantitative statistical analyses of 2D NMR lineshapes obtained from through-space correlation experiments acquired at variable mixing times. Low-energy vibration modes calculated from first principles can be conveniently used to generate a plausible basis set of physically realistic local distortions as candidates to describe the static distributions of local geometries that are responsible for the disorder. Predicted 2D correlation lineshapes simulated from calculations of NMR chemical shifts carried out for the different sets of candidate distortions can then be compared to the experimental 2D isotropic chemical shift distributions, thereby allowing the unambiguous elimination of the structural distortions that are not compatible with the local structural disorder. In the particular case of the "crystalline" bisphosphinoamine studied here, we have thus been able to demonstrate the presence of small amplitude structural disorder and to establish the spatial range of this disorder to be less than ca. 1 nm. We have identified at least one type of structural deformation that is compatible with the experimental 2D NMR data and is also within the order of magnitude of the "thermal ellipsoids" associated with the uncertainties on the atomic positions of the X-ray diffraction structure. These results highlight the extreme sensitivity of NMR chemical shifts to structural variations, since the disorder examined here is clearly visible on the spectrum, yet corresponds to variations of a couple of degrees in bond and dihedral angles. Similar analyses using a full solid-state treatment with plane-wave-based DFT methods[43,44,59,60] would intrinsically account for intermolecular effects such as ring currents or hydrogen bonding in solids where they are expected to contribute to disorder and the resulting distributions of NMR chemical shifts.[81,85−87] The general approach presented here should be applicable to a broad range of solids with small amplitude structural disorder and will ultimately allow us to link this type of disorder to their macroscopic physical and chemical properties.

Acknowledgment. Solid-state NMR spectra were recorded at the Rhône-Alpes Large Scale Facility for NMR (http://www.ralf-nmr.fr/). S.C. and P.S. thank IDRIS (project 070609) and PSMN for the attribution of CPU time. We are grateful to Dr. Niklas Hedin (Stockholm, Sweden) and Dr. David Loffreda (Lyon, France) for stimulating discussions, and to Dr. Michel Bardet and Dr. Yves Gimbert (Grenoble, France) for providing us with the bisphosphinoamine sample.

Supporting Information Available: Calculation of the ^{31}P−^{14}N second-order dipole−quadrupole interactions. Procedures for the extraction of conditional probability matrices and for the calculation of degrees of chemical shift correlation r_{AB} and of Pearson product-moment coefficients ρ_{AB}. Figure S1: complete series of ^{31}P−^{31}P spin diffusion spectra, recorded at mixing times ranging between 5 ms and 2 s. This material is available free of charge via the Internet at http://pubs.acs.org.

References and Notes

(1) Farnan, I.; Grandinetti, P. J.; Baltisberger, J. H.; Stebbins, J. F.; Werner, U.; Eastman, M. A.; Pines, A. *Nature* **1992**, *358*, 31–35.
(2) Schmidt-Rohr, K.; Spiess, H. W. *Multi-dimensional solid-state NMR and polymers*; Academic Press: San Diego, 1994.
(3) Youngman, R. E.; Haubrich, S. T.; Zwanziger, J. W.; Janicke, M. T.; Chmelka, B. F. *Science* **1995**, *269*, 1416–1420.
(4) Stebbins, J. F.; Xu, Z. *Nature* **1997**, *390*, 60–62.
(5) Samoson, A.; Lippmaa, E.; Pines, A. *Mol. Phys.* **1988**, *65*, 1013–1018.
(6) Llor, A.; Virlet, J. *Chem. Phys. Lett.* **1988**, *152*, 248–253.
(7) Chmelka, B. F.; Mueller, K. T.; Pines, A.; Stebbins, J.; Wu, Y.; Zwanziger, J. W. *Nature* **1989**, *339*, 42–43.
(8) Medek, A.; Harwood, J. S.; Frydman, L. *J. Am. Chem. Soc.* **1995**, *117*, 12779–12787.
(9) Frydman, L.; Harwood, J. S. *J. Am. Chem. Soc.* **1995**, *117*, 5367–5368.
(10) Gan, Z. H. *J. Am. Chem. Soc.* **2000**, *122*, 3242–3243.

(11) Frydman, L. In *Encyclopedia of Nuclear Magnetic Resonance*; Grant, D. M., Harris, R. K., Eds.; Wiley: Chichester, 2002; Vol. *9*, p 262.
(12) Amoureux, J. P.; Pruski, M. In *Encyclopedia of Nuclear Magnetic Resonance*; Grant, D. M., Harris, R. K., Eds.; Wiley: Chichester, 2002; Vol. 9, p 226.
(13) Jerschow, A. *Prog. Nucl. Magn. Reson. Spectrosc.* **2005**, *46*, 63–78.
(14) Mackenzie, K. J. D.; Smith, M. E. *Multinuclear solid-state NMR of inorganic materials*; Pergamon Press: Oxford, 2002.
(15) Allwardt, J. R.; Lee, S. K.; Stebbins, J. F. *Am. Mineral.* **2003**, *88*, 949–954.
(16) Iuga, D.; Morais, C.; Gan, Z. H.; Neuville, D. R.; Cormier, L.; Massiot, D. *J. Am. Chem. Soc.* **2005**, *127*, 11540–11541.
(17) Allwardt, J. R.; Stebbins, J. F.; Schmidt, B. C.; Frost, D. J.; Withers, A. C.; Hirschmann, M. M. *Am. Mineral.* **2005**, *90*, 1218–1222.
(18) Neuville, D. R.; Cormier, L.; Montouillout, V.; Massiot, D. *J. Non-Cryst. Solids* **2007**, *353*, 180–184.
(19) Massiot, D.; Fayon, F.; Montouillout, V.; Pellerin, N.; Hiet, J.; Roiland, C.; Florian, P.; Coutures, J. P.; Cormier, L.; Neuville, D. R. *J. Non Cryst. Solids* **2008**, *354*, 249–254.
(20) Janicke, M. T.; Landry, C. C.; Christiansen, S. C.; Kumar, D.; Stucky, G. D.; Chmelka, B. F. *J. Am. Chem. Soc.* **1998**, *120*, 6940–6951.
(21) Babonneau, F.; Maquet, J. *Polyhedron* **2000**, *19*, 315–322.
(22) Trebosc, J.; Wiench, J. W.; Huh, S.; Lin, V. S. Y.; Pruski, M. *J. Am. Chem. Soc.* **2005**, *127*, 7587–7593.
(23) Sefzik, T. H.; Houseknecht, J. B.; Clark, T. M.; Prasad, S.; Lowary, T. L.; Gan, Z.; Grandinetti, P. J. *Chem. Phys. Lett.* **2007**, *434*, 312–315.
(24) Maricq, M. M.; Waugh, J. S. *J. Chem. Phys.* **1979**, *70*, 3300–3316.
(25) Deschamps, M.; Fayon, F.; Hiet, J.; Ferru, G.; Derieppe, M.; Pellerin, N.; Massiot, D. *Phys. Chem. Chem. Phys.* **2008**, *10*, 1298−1303.
(26) Christiansen, S. C.; Zhao, D. Y.; Janicke, M. T.; Landry, C. C.; Stucky, G. D.; Chmelka, B. F. *J. Am. Chem. Soc.* **2001**, *123*, 4519–4529.
(27) Sakellariou, D.; Brown, S. P.; Lesage, A.; Hediger, S.; Bardet, M.; Meriles, C. A.; Pines, A.; Emsley, L. *J. Am. Chem. Soc.* **2003**, *125*, 4376–4380.
(28) Hedin, N.; Graf, R.; Christiansen, S. C.; Gervais, C.; Hayward, R. C.; Eckert, J.; Chmelka, B. F. *J. Am. Chem. Soc.* **2004**, *126*, 9425–9432.
(29) Cadars, S.; Lesage, A.; Emsley, L. *J. Am. Chem. Soc.* **2005**, *127*, 4466–4476.
(30) Cadars, S.; Lesage, A.; Trierweiler, M.; Heux, L.; Emsley, L. *Phys. Chem. Chem. Phys.* **2007**, *9*, 92–103.
(31) Cadars, S.; Mifsud, N.; Lesage, A.; Epping, J. D.; Hedin, N.; Chmelka, B. F.; Emsley, L. *J. Phys. Chem. C* **2008**, *112*, 9145–9154.
(32) Marcotte, I.; van Beek, J. D.; Meier, B. H. *Macromolecules* **2007**, *40*, 1995–2001.
(33) Vander Hart, D. L. In *Encyclopedia of NMR*; Grant, D. M., Harris, R. K., Eds.; Wiley: Chichester, 1996; Vol. 5, pp 2938−2946.
(34) Spaniol, T. P.; Kubo, A.; Terao, T. *Mol. Phys.* **1999**, *96*, 827–834.
(35) Kervern, G.; Pintacuda, G.; Zhang, Y.; Oldfield, E.; Roukoss, C.; Kuntz, E.; Herdtweck, E.; Basset, J. M.; Cadars, S.; Lesage, A.; Coperet, C.; Emsley, L. *J. Am. Chem. Soc.* **2006**, *128*, 13545–13552.
(36) Zhang, P.; Klymachyov, A.; Brown, S.; Ellington, J. G.; Grandinetti, P. J. *Solid State Nucl. Magn. Reson.* **1998**, *12*, 221–225.
(37) Charpentier, T.; Ispas, S.; Profeta, M.; Mauri, F.; Pickard, C. J. *J. Phys. Chem. B* **2004**, *108*, 4147–4161.
(38) Clark, T. M.; Grandinetti, P. J. *J. Phys.: Condens. Matter* **2003**, *15*, S2387–S2395.
(39) Clark, T. M.; Grandinetti, P. J.; Florian, P.; Stebbins, J. F. *Phys. Rev. B* **2004**, *70*, 064202.
(40) Schmidt-Rohr, K.; Hehn, M.; Schaefer, D.; Spiess, H. W. *J. Chem. Phys.* **1992**, *97*, 2247–2262.
(41) Schmidt-Rohr, K.; Hu, W.; Zumbulyadis, N. *Science* **1998**, *280*, 714–717.
(42) Pickard, C. J.; Mauri, F. *Phys. Rev. B* **2001**, *63*, 245101.
(43) Sebastiani, D.; Parrinello, M. *J. Phys. Chem. A* **2001**, *105*, 1951–1958.
(44) Sebastiani, D.; Goward, G.; Schnell, I.; Parrinello, M. *Comput. Phys. Commun.* **2002**, *147*, 707–710.
(45) Yates, J. R.; Pickard, C. J.; Mauri, F. *Phys. Rev. B* **2007**, *76*, 024401.
(46) Tielens, F.; Gervais, C.; Lambert, J. F.; Mauri, F.; Costa, D. *Chem. Mater.* **2008**, *20*, 3336–3344.
(47) Gimbert, Y.; Robert, F.; Durif, A.; Averbuch, M. T.; Kann, N.; Greene, A. E. *J. Org. Chem.* **1999**, *64*, 3492–3497.
(48) Konya, D.; Robert, F.; Gimbert, Y.; Greene, A. E. *Tetrahedron Lett.* **2004**, *45*, 6975–6978.
(49) Hediger, S.; Meier, B. H.; Kurur, N. D.; Bodenhausen, G.; Ernst, R. R. *Chem. Phys. Lett.* **1994**, *223*, 283–288.
(50) Fung, B. M.; Khitrin, A. K.; Ermolaev, K. *J. Magn. Reson.* **2000**, *142*, 97–101.
(51) van Beek, J. D. *J. Magn. Reson.* **2007**, *187*, 19–26.
(52) Frisch, M. J.; Trucks, G. W.; Schlegel, H. B.; Scuseria, G. E.; Robb, M. A.; Cheeseman, J. R.; Montgomery, J., J. A.; Vreven, T.; Kudin, K. N.; Burant, J. C.; Millam, J. M.; Iyengar, S. S.; Tomasi, J.; Barone, V.; Mennucci, B.; Cossi, M.; Scalmani, G.; Rega, N.; Petersson, G. A.; Nakatsuji, H.; Hada, M.; Ehara, M.; Toyota, K.; Fukuda, R.; Hasegawa, J.; Ishida, M.; Nakajima, T.; Honda, Y.; Kitao, O.; Nakai, H.; Klene, M.; Li, X.; Knox, J. E.; Hratchian, H. P.; Cross, J. B.; Bakken, V.; Adamo, C.; Jaramillo, J.; Gomperts, R.; Stratmann, R. E.; Yazyev, O.; Austin, A. J.; Cammi, R.; Pomelli, C.; Ochterski, J. W.; Ayala, P. Y.; Morokuma, K.; Voth, G. A.; Salvador, P.; Dannenberg, J. J.; Zakrzewski, V. G.; Dapprich, S.; Daniels, A. D.; Strain, M. C.; Farkas, O.; Malick, D. K.; Rabuck, A. D.; Raghavachari, K.; Foresman, J. B.; Ortiz, J. V.; Cui, Q.; Baboul, A. G.; Clifford, S.; Cioslowski, J.; Stefanov, B. B.; Liu, G.; Liashenko, A.; Piskorz, P.; Komaromi, I.; Martin, R. L.; Fox, D. J.; Keith, T.; Al-Laham, M. A.; Peng, C. Y.; Nanayakkara, A.; Challacombe, M.; Gill, P. M. W.; Johnson, B.; Chen, W.; Wong, M. W.; Gonzalez, C.; Pople, J. A. Gaussian 03, Revision D.01, Gaussian, Inc., Wallingford CT, 2004.
(53) Becke, A. D. *J. Chem. Phys.* **1993**, *98*, 5648–5652.
(54) Perdew, J. P.; Yue, W. *Phys. Rev. B* **1986**, *33*, 8800–8802.
(55) Lee, C. T.; Yang, W. T.; Parr, R. G. *Phys. Rev. B* **1988**, *37*, 785–789.
(56) Ziegler, T. *Chem. Rev.* **1991**, *91*, 651–667.
(57) Feller, D. *J. Comput. Chem.* **1996**, *17*, 1571–1586.
(58) Schuchardt, K. L.; Didier, B. T.; Elsethagen, T.; Sun, L. S.; Gurumoorthi, V.; Chase, J.; Li, J.; Windus, T. L. *J. Chem Inf. Model.* **2007**, *47*, 1045–1052.
(59) Segall, M. D.; Lindan, P. J. D.; Probert, M. J.; Pickard, C. J.; Hasnip, P. J.; Clark, S. J.; Payne, M. C. *J. Phys.: Condens. Matter* **2002**, *14*, 2717–2744.
(60) Clark, S. J.; Segall, M. D.; Pickard, C. J.; Hasnip, P. J.; Probert, M. J.; Refson, K.; Payne, M. C. *Z. Kristallogr.* **2005**, *220*, 567–570.
(61) Perdew, J. P.; Burke, K.; Ernzerhof, M. *Phys. Rev. Lett.* **1996**, *77*, 3865–3868.
(62) Vanderbilt, D. *Phys. Rev. B* **1990**, *41*, 7892–7895.
(63) Monkhorst, H. J.; Pack, J. D. *Phys. Rev. B* **1976**, *13*, 5188–5192.
(64) Robert, F.; Gimbert, Y.; Averbuch-Pouchot, M. T.; Greene, A. E. *Z. Krist.-New Cryst. Struct.* **2000**, *215*, 233–236.
(65) Lesage, A.; Bardet, M.; Emsley, L. *J. Am. Chem. Soc.* **1999**, *121*, 10987–10993.
(66) deDios, A. C. *Prog. Nucl. Magn. Reson. Spectrosc.* **1996**, *29*, 229–278.
(67) Bull, L. M.; Bussemer, B.; Anupold, T.; Reinhold, A.; Samoson, A.; Sauer, J.; Cheetham, A. K.; Dupree, R. *J. Am. Chem. Soc.* **2000**, *122*, 4948–4958.
(68) Xue, X. Y.; Kanzaki, M. *Solid State Nucl. Magn. Reson.* **2000**, *16*, 245–259.
(69) Gervais, C.; Profeta, M.; Babonneau, F.; Pickard, C. J.; Mauri, F. *J. Phys. Chem. B* **2004**, *108*, 13249–13253.
(70) Yates, J. R.; Dobbins, S. E.; Pickard, C. J.; Mauri, F.; Ghi, P. Y.; Harris, R. K. *Phys. Chem. Chem. Phys.* **2005**, *7*, 1402–1407.
(71) Yates, J. R.; Pham, T. N.; Pickard, C. J.; Mauri, F.; Amado, A. M.; Gil, A. M.; Brown, S. P. *J. Am. Chem. Soc.* **2005**, *127*, 10216–10220.
(72) Harris, R. K.; Joyce, S. A.; Pickard, C. J.; Cadars, S.; Emsley, L. *Phys. Chem. Chem. Phys.* **2006**, *8*, 137–143.
(73) Mifsud, N.; Elena, B.; Pickard, C. J.; Lesage, A.; Emsley, L. *Phys. Chem. Chem. Phys.* **2006**, *8*, 3418–3422.
(74) Ashbrook, S. E.; Berry, A. J.; Frost, D. J.; Gregorovic, A.; Pickard, C. J.; Readman, J. E.; Wimperis, S. *J. Am. Chem. Soc.* **2007**, *129*, 13213–13224.
(75) Harris, R. K.; Cadars, S.; Emsley, L.; Yates, J. R.; Pickard, C. J.; Jetti, R. K. R.; Griesser, U. J. *Phys. Chem. Chem. Phys.* **2007**, *9*, 360–368.
(76) Pickard, C. J.; Salager, E.; Pintacuda, G.; Elena, B.; Emsley, L. *J. Am. Chem. Soc.* **2007**, *129*, 8932–8933.
(77) Brouwer, D. H. *J. Am. Chem. Soc.* **2008**, *130*, 6306–6307.
(78) Brouwer, D. H. *J. Magn. Reson.* **2008**, *194*, 136−146.
(79) Harris, R. K.; Hodgkinson, P.; Pickard, C. J.; Yates, J. R.; Zorin, V. *Magn. Reson. Chem.* **2007**, *45*, S174–S186.
(80) Lazzeretti, P. *Prog. Nucl. Magn. Reson. Spectrosc.* **2000**, *36*, 1–88.
(81) Brown, S. P.; Spiess, H. W. *Chem. Rev.* **2001**, *101*, 4125–4155.
(82) Harris, R. K.; Olivieri, A. C. *Prog. Nucl. Magn. Reson. Spectrosc.* **1992**, *24*, 435–456.
(83) Hedin, N., personal communication.
(84) Cohen, J.; West, S. G.; Cohen, P.; Aiken, L. S. *Applied multiple regression/correlation analysis for the behavioral sciences*, 3rd ed.; Lawrence Erlbaum Assoc. Inc.: Hillsdale, NJ, 2003.
(85) Percec, V.; Glodde, M.; Bera, T. K.; Miura, Y.; Shiyanovskaya, I.; Singer, K. D.; Balagurusamy, V. S. K.; Heiney, P. A.; Schnell, I.; Rapp, A.; Spiess, H. W.; Hudson, S. D.; Duan, H. *Nature* **2002**, *419*, 384–387.
(86) Goward, G. R.; Sebastiani, D.; Schnell, I.; Spiess, H. W.; Kim, H. D.; Ishida, H. *J. Am. Chem. Soc.* **2003**, *125*, 5792–5800.
(87) Schmidt, J.; Hoffmann, A.; Spiess, H. W.; Sebastiani, D. *J. Phys. Chem. B* **2006**, *110*, 23204–23210.

JP810138Y